



HAL
open science

Measurement of pore size distribution of building materials by thermal method

Nicolas Dujardin, Thouraya Salem, Vincent Feuillet, Magali Fois, Laurent Ibos, Christophe Poilâne, Rémi Manuel

► To cite this version:

Nicolas Dujardin, Thouraya Salem, Vincent Feuillet, Magali Fois, Laurent Ibos, et al.. Measurement of pore size distribution of building materials by thermal method. *Construction and Building Materials*, 2020, 245, pp.118417. 10.1016/j.conbuildmat.2020.118417 . hal-03348177

HAL Id: hal-03348177

<https://hal.science/hal-03348177>

Submitted on 22 Aug 2022

HAL is a multi-disciplinary open access archive for the deposit and dissemination of scientific research documents, whether they are published or not. The documents may come from teaching and research institutions in France or abroad, or from public or private research centers.

L'archive ouverte pluridisciplinaire **HAL**, est destinée au dépôt et à la diffusion de documents scientifiques de niveau recherche, publiés ou non, émanant des établissements d'enseignement et de recherche français ou étrangers, des laboratoires publics ou privés.



Distributed under a Creative Commons Attribution - NonCommercial 4.0 International License

Measurement of pore size distribution of building materials by thermal method

Nicolas DUJARDIN^{1*}, Thouraya SALEM¹, Vincent FEUILLET¹, Magali FOIS¹, Laurent IBOS¹, C. POILANE², Rémi MANUEL³

¹CERTES, OSU-Efluve, Université Paris-Est, 94010 Cedex
*(corresponding author : nicolas.dujardin@u-pec.fr)

² CIMAP, Alençon Site Universitaire de Montfoulon, 61250 Damigny

³ Centre d'études et de recherche en mécanique et automatismes, Université d'Evry
40, rue du Pelvoux – 91020 Courcouronnes

Abstract

The present work focuses on the study of the thermophysical properties of low porous insulation materials. In peculiar, we investigate the pore structure of composite materials and cements by thermal method. This method, adapted for fragile materials, is based on an existing model which allows the determination of pore size distribution. Firstly, the existing analytical model is presented. The thermal conductivity is modeled by assimilating the studied medium to N fluid phases and one solid phase in series / parallel. Secondly, some extensions to this model are proposed. In particular, we show that in the case of a single pore size, it is possible to obtain a finer pore size distribution by means of a normal law. We also show for the first time that the normalization of the thermal conductivity is an interesting way to study the pore size distribution of a material without knowing the overall porosity rate (which strongly depends on the method used). Furthermore, this model and its extensions have been successfully applied to different kinds of materials (plant fiber composites and cements). Fibers reinforced composites have one class of pores around 30 – 60 μm . Chemical treatments do not affect this pore size. Cements show a macroporosity (around 20 μm) which is often underestimated.

Keywords: porosity, thermal conductivity, modelling, composite, cement, chemical treatments

Nomenclature

C Constant depending on gas nature ($\text{Pa}\cdot\text{m}\cdot\text{K}^{-1}$)
d Pore size (m)
P Pressure (Pa)
T Temperature (K)

Greek letters

α Fraction of the gas in the continuous path
 β Fraction of the solid in the continuous path

ε_x	Volume fraction of the x phase
λ	Thermal conductivity ($\text{W}\cdot\text{m}^{-1}\cdot\text{K}^{-1}$)
σ	Standard deviation of the normal law

Subscripts

air	Air
atm	Atmospheric pressure
i	i^{th} air phase
est	Estimated
mes	Measured
norm	Normalized
s	Solid phase
sec	Secondary pressure (vacuum)

1. Introduction

The start of the 21st century was marked by general awareness of the need to limit the impact of human activity on the environment. Even if, as the outcome of the recent world climate summit shows from Madrid, we are still far from an international consensus on the means to implement to achieve this goal, it is no longer possible to ignore the incentives and the constraints that push the integration of projects, whatever the sector of activity, to a sustainable development approach. As far as the building sector is concerned, it must work to convert its practices to improve the energy performance of new and existing buildings but also to offer innovative materials that meet the new requirements of legislation in terms of environmental and health impact.

Porosity is a main parameter in insulation materials. Its presence is inherent to the manufacturing process and sometimes to the material itself. Thus, the porosity must be reduced to a minimum for some applications [1] whereas in other cases, high and optimal porosity is sought such as for insulation materials [2].

Table 1 shows a summary of several techniques used to determine porosity. It shows that each technique probes only a specific pore size. Most of techniques are destructive as the most widely used: Mercury Intrusion Porosimetry (MIP). Others, as thermal methods, are non-destructive. No technique is able to adequately characterize the entire network of pore sizes leading to an inaccurate picture of porosity. For example, MIP provides access to several decades of pore size, nevertheless there are several problems. Firstly, at low pressure, the pores likely to take part in the constitution of the penetration paths are few (shallow invasion). Secondly, when the pressure increases a percolation phenomenon occurs from a critical diameter [3].

chemical treatment. But those of the three other samples all underwent a chemical treatment: leaching (attack with weakly concentrated NaOH), bleaching (attack with H₂O₂) or mercerization (attack with strongly concentrated NaOH). These composites have an overall porosity between 10 and 15% (deduced from the fabric basic weight, the number of layers in the laminate, the fiber density and the resin density [18]).

Two types of concrete have been studied: in the first one the ordinary Portland Cement CEM I was used and in the second one the ultra-high performance fiber concrete, named UHPC was used. The water-to-cement ratio (w/c) was 0.5 for CEM I and 0.24 for UHPC. CEM I and UHPC have an overall porosity respectively of 30% and 4%. Prior to the thermal characterization, the samples were dried under secondary vacuum for 15 days. The removal of water using drying may damage the pore structure of cement based materials [19-22]. This water removal technique was chosen because it is one of the methods that affects less the microstructure.

2.2 Thermal characterization method (modified DICO experiment)

As said in the introduction, the aim of the paper is to characterize the porosity of heterogeneous materials using a thermal method. Therefore, all samples were characterized using an existing setup (DICO) previously described in references [17, 23]. Some modifications were done to the vacuum pumping system in order to be able to fix the pressure value in the experiment between atmospheric pressure and secondary vacuum domain, by means of two pumps and micro-leaks. Thus, this system makes possible the characterization of pore sizes ranging from 100 nm to 1 mm.

The technique is based on a periodic thermal excitation regime [17]. Figure 1 shows a block diagram of the experimental setup. A plate-like sample of 44 mm side and a few millimeters thick is placed between two metallic plates in the vacuum chamber. Two K-type thermocouples are inserted in these metallic plates allowing to measure changes in the temperature on the front and rear faces of the sample, namely T₁ and T₂ (see Figure 1). Both K-type thermocouples are connected to a data acquisition device controlled by a LabView™ application. The excitation signal is periodic (superposition of a sum of five harmonics) and imposed by a thermoelectric cooler (Peltier cell) fixed below the sample holder [23].

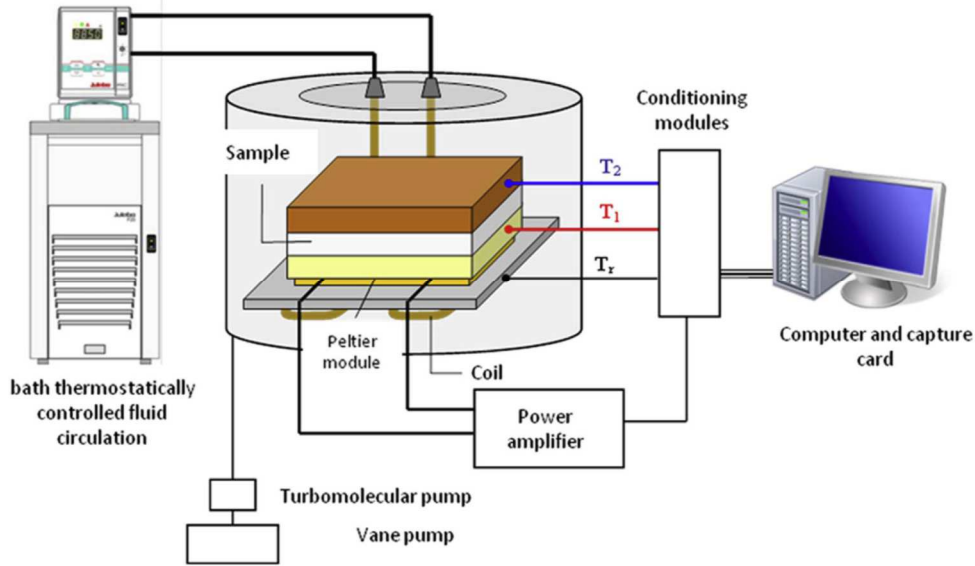


Figure 1. Block diagram of the “DICO” experimental setup [23].

The experimental transfer function is calculated from the measured plates temperatures and the theoretical transfer function is determined by the thermal quadrupole method. Thermal conductivity and diffusivity are simultaneously identified from the real and imaginary parts of these transfer functions [17]. This method also provides the statistical uncertainties of these two quantities.

3. Modeling

3.1 Thermal conductivity model

3.1.1 Thermal conductivity of the air

A porous material is composed of air whose effective thermal conductivity depends both on its pressure, the pore size in which it is contained and the temperature. With the DICO device, the excitation signal leads to an increase of a few degrees in the temperature at each frequency ($\Delta T_{\max} = 10$ K). As such an increase induces 0.02 % of variation in the conductivity of the air (for $d = 10$ μm), the effect of temperature can be neglected.

As a result, the pore size and the pressure are the important parameters in the equation of the thermal conductivity of air that is confined in a pore. The variation of the thermal conductivity of the air as a function of pressure is governed by the Knudsen effect, according to which:

$$\lambda_{air} = \frac{\lambda_{air,atm}}{1 + C\left(\frac{T}{Pd}\right)} \quad (1)$$

where $\lambda_{air,atm}$ is thermal conductivity of the air at atmospheric pressure and ambient temperature (0.026 $\text{W}\cdot\text{m}^{-1}\cdot\text{K}^{-1}$ at 300 K) [11]; T is the temperature (K); P is the air pressure

(Pa); C is a constant depending on the gas nature ($C = 2.5 \times 10^{-5} \text{ Pa}\cdot\text{m}\cdot\text{K}^{-1}$) [24]; and d is the pore size (m).

Figure 2 shows the variation of the thermal conductivity of a porous material as a function of pressure for different pore sizes. It clearly shows that the thermal conductivity of air strongly depends on the pore size over this pressure range. In particular, the smaller pores are the most insulating.

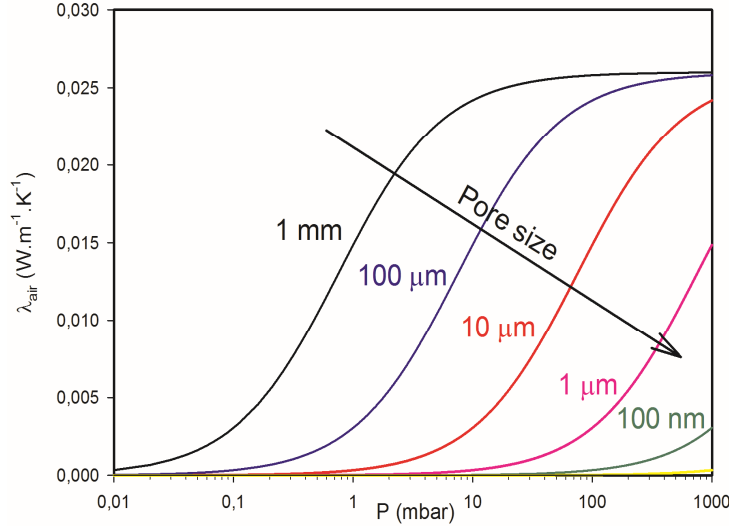


Figure 2. Thermal conductivity of the air as a function of pressure for different pore sizes (at 300 K).

3.1.2. Thermal conductivity of heterogeneous media

Several models can be used to predict the effective thermal conductivity of heterogeneous media (parallel, Bruggeman, Maxwell, *etc.*). Among them, the combined serial/parallel model on which this study is based has been developed by Félix *et al.* [11]. This approach consists in considering a heterogeneous medium of porosity $\epsilon_{\text{air}} = 1 - \epsilon_s$ whose solid phase has a conductivity λ_s and whose fluid phase is air of conductivity λ_{air} . A fraction β of the solid phase and α of the fluid phase are considered in a strictly parallel model, of equivalent thermal conductivity λ_1 . The remaining fractions $(1 - \beta)$ and $(1 - \alpha)$ are also put in parallel (equivalent conductivity λ_2). Serialization of λ_1 and λ_2 leads to equation 2 which gives the expression of the equivalent thermal conductivity of the medium for one solid phase and N fluid phases. Figure 3 shows a schematic representation of this model.

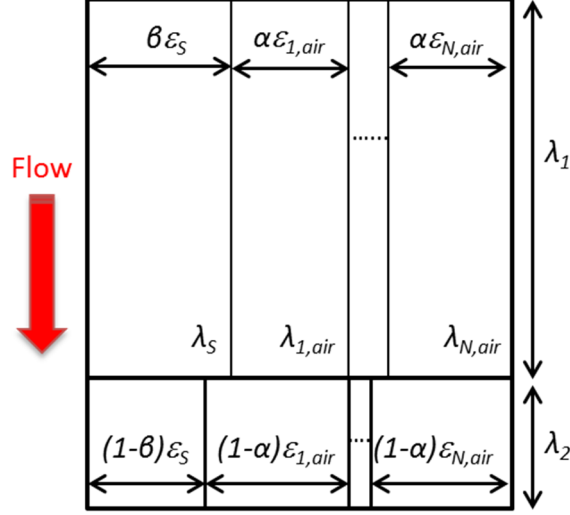


Figure 3. Schematic representation of the serial-parallel model for $(N + 1)$ phases (adapted from [11]).

The effective thermal conductivity of the material is [11]:

$$\lambda = \frac{1}{\frac{\beta\varepsilon_s + \alpha(1-\varepsilon_s)}{\lambda_1} + \frac{(1-\beta)\varepsilon_s + (1-\alpha)(1-\varepsilon_s)}{\lambda_2}} \quad (2)$$

with conductivities λ_1 and λ_2 are calculated using a discrete distribution of $\lambda_{i,air}$:

$$\lambda_1 = \frac{\beta\varepsilon_s\lambda_s + \alpha\sum_{i=1}^N \varepsilon_{i,air}\lambda_{i,air}}{\beta\varepsilon_s + \alpha(1-\varepsilon_s)} \quad \text{et} \quad \lambda_2 = \frac{(1-\beta)\varepsilon_s\lambda_s + (1-\alpha)\sum_{i=1}^N \varepsilon_{i,air}\lambda_{i,air}}{(1-\beta)\varepsilon_s + (1-\alpha)(1-\varepsilon_s)} \quad (3)$$

3.2 Model extensions

Extensions to the model proposed by Félix *et al.* [11] have been made. Thus, in the case of a single pore size (unimodal distribution), a size distribution according to a normal law is proposed. Then, since knowledge of the overall porosity rate can be tricky, we propose to normalize the thermal conductivity to determine the pore size distribution without the need for this data.

3.2.1 Unimodal distribution

The above approach proposed by Félix *et al.* [11] is based on *a priori* knowledge of the different pore sizes $d_{i,air}$ characterizing the material for the calculation of conductivities $\lambda_{i,air}$ from equation (1). However, the material studied can in some cases exhibit an unimodal behavior. In this case, a normal law is proposed to express the volume fraction ε according to the pore size d in the form:

$$\varepsilon_{i,air} = \Delta d \frac{1}{\sigma\sqrt{2\pi}} \exp\left\{-0.5\left[\frac{(d_i - d_{moy})}{\sigma}\right]^2\right\} \varepsilon_{air} \quad \text{with } d_i \text{ varying from } d_{min} \text{ to } d_{max} \quad (4)$$

where Δd is the step of discretization of the pore size, σ the standard deviation of the normal law, d_{moy} the average pore size of the normal law and ε_{air} the overall rate of porosity. This approach makes it possible for the samples concerned to obtain a finer distribution of the pore size.

The parameter Δd is chosen equal to 50 nm which allows a good compromise between computation time and accuracy of the profile of volume fraction obtained. d_{min} and d_{max} are respectively equal to 0.01 nm and 500 μm , which makes it possible to consider a wide range of possible pore sizes. The corresponding thermal conductivity can then be calculated at each pressure level using equations (1), (3) and (2).

3.2.2 Normalization

Assuming known the overall porosity rate, the model, as it currently exists, allows the identification of the pore size distribution by minimizing the quadratic difference between the measured and the simulated thermal conductivities. The knowledge of the overall porosity rate is decisive because the thermal conductivity values depend on it, as shown in Figure 4.

In practice, the porosity rate is not always known and, when it is, is dependent on the method used [16]. In order to overcome this initial data, it is possible to normalize the thermal conductivity λ_{norm} values between 0 and 1:

$$\lambda_{norm} = \frac{\lambda_P - \lambda_{P_{sec}}}{\lambda_{P_{atm}} - \lambda_{P_{sec}}} \quad (5)$$

where λ_P , $\lambda_{P_{sec}}$ and $\lambda_{P_{atm}}$ are the measured thermal conductivity respectively at pressure P, in secondary vacuum domain and at atmospheric pressure. Such a normalization has already been done but not for that purpose. Jannot et al. [25] used it to show that reduced thermal conductivities of 8 estimation models of thermal conductivity almost superimposed for high porous materials whatever the model. They did not discuss about the overall porosity rate.

When normalizing the thermal conductivity, as shown in Figure 5, the thermal conductivity curves as a function of pressure are superimposed regardless of the overall porosity rate. Thus, this is a very interesting way to overcome the knowledge of this parameter.

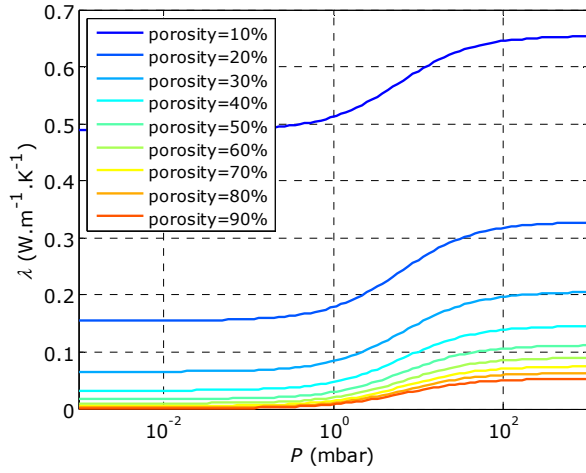


Figure 4. Variation of the thermal conductivity of the air as a function of the pressure for different global porosity rates ($d = 10 \mu\text{m}$).

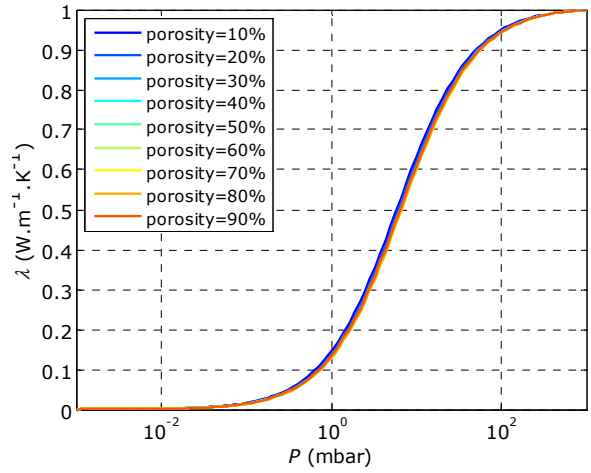


Figure 5. Normalized conductivity as a function of pressure for different porosity rates.

3.3 Adjustment of the model

The adjustment to the measurement was carried out by minimizing the criterion of equation (6) using the Levenberg-Marquardt algorithm [26]:

$$S = \sum_{j=1}^J \left[\lambda_{mes}^j - \lambda_{est}^j(p) \right]^2 \quad (6)$$

where λ_{mes} are the measured conductivities, λ_{est} are the estimated conductivities calculated using the model (see sections 3.1 for the combined serial-parallel model and 3.2.1 for the normal law), j is the number of experimental data and p is the vector of parameters to be estimated. In the case of the model of the equations (2) and (3), the parameters of the vector p are : α , β , λ_s and the volume fractions $\varepsilon_{i, air}$. In the case of the application of the normal law of equation (4), these parameters are: α , β , λ_s , d_{moy} and σ .

Estimated parameters are initialized to realistic values, the minimization algorithm has been shown to be insensitive to these initial values. A sensitivity analysis carried out in [11] showed that the optimal number of pore sizes to be considered for the model of equations (2) and (3) is 5, between the hundred nanometers to one millimeter.

4. Results and discussion

4.1 Plant fibers composites

Figure 6a shows the variation of the thermal conductivity as a function of pressure for a composite based on plant fibers.

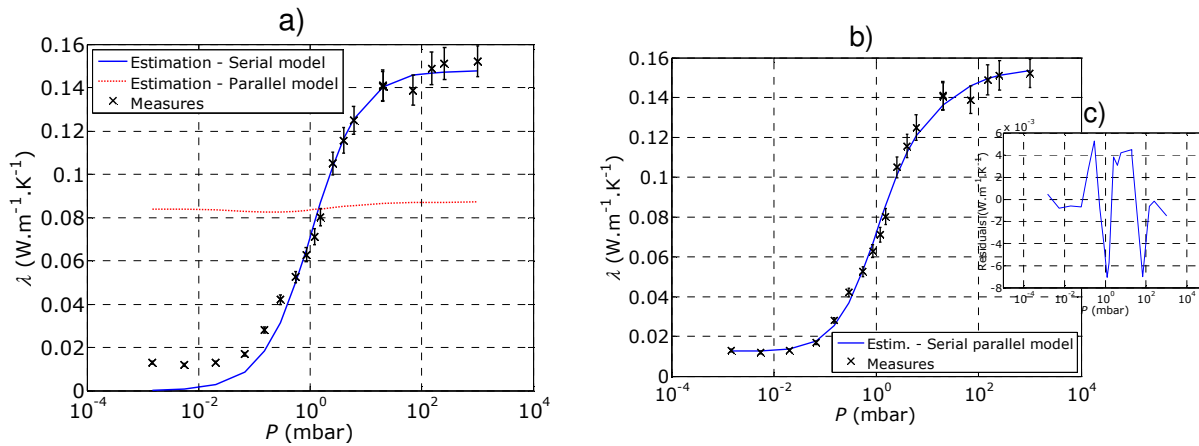


Figure 6. Comparison of the measured and estimated thermal conductivities of the bleached composite

a) Estimations with serial and parallel models; b) Estimation with combined serial-parallel model; c) Residuals for estimation with combined serial-parallel model

The variation in thermal conductivity is significant (one decade), showing the porous nature of the material. To adjust the experimental curve, we used three different models: parallel, serial and the serial-parallel model developed by Felix *et al.* for very porous materials ($\sim 90\%$) [11]. It appears that only this model perfectly fits the experimental curve (cf. residuals figure 6b) which corroborates this assessment according to which for low porous materials the models of thermal conductivity are not equivalent anymore [25]. Thus, the CSP model and can therefore be transposed to low porosity materials (10-15%).

This model provides access to the pore size distribution within this composite. It clearly indicates a single class of pore size, approximately $20 \mu\text{m}$ (Figure 7). In the literature, the porosity in this type of composites is rather approached in terms of volume [18, 27, 28] than in terms of size. Thus, although the porosity may have several origins (fiber porosity, porosity interface, impregnation porosity, matrix porosity) and therefore potentially several sizes, these are rarely discussed [29-31]. However, the value of $20 \mu\text{m}$ determined in this study is an intermediate value between the porosity of the fiber (the lumen of few microns) and the porosity of impregnation or internal to the matrix which can reach a few tens of microns) [30].

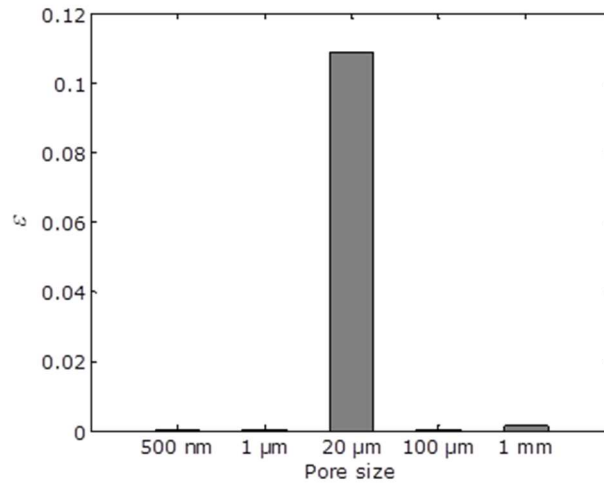


Figure 7. Estimation of the pore size distribution from the serial-parallel model.

As the results indicate a unimodal distribution of pore sizes, the pore size distribution can be refined around this mean value using the normal law model (Figure 8). In this case, the average pore size for the bleached sample is estimated at $40 \mu\text{m}$ with a standard deviation of $33 \mu\text{m}$.

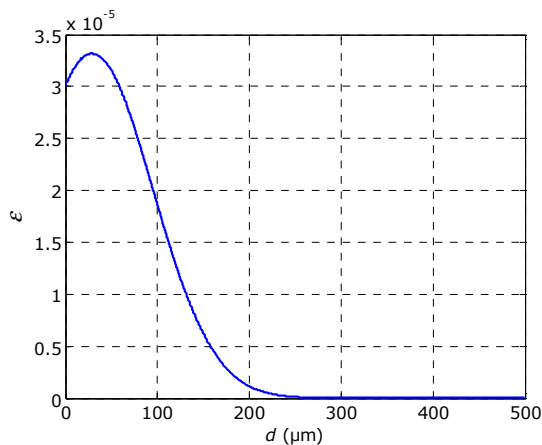


Figure 8. Volume fraction versus normal pore size for the bleached composite from the normal law model.

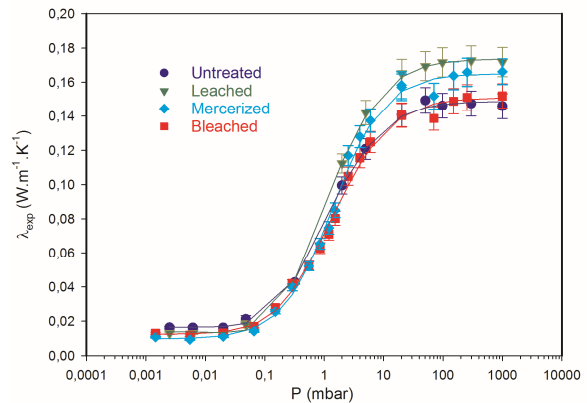


Figure 9. Measured and estimated thermal conductivity versus pressure for each composite.

Figure 9 shows the variations of the measured and estimated thermal conductivity of composites reinforced by natural fibers. Whatever the chemical treatment of fibers, the thermal conductivities of each composite are superimposed on almost the entire pressure range.

	Untreated	Leached	Bleached	Mercerised
$d_{\text{moy}} (\mu\text{m})$	54	51	40	56
$\sigma (\mu\text{m})$	35	32	33	25

Table 2. Average pore size and standard deviation obtained by the normal law for lin/epoxy composites.

The normal law model was applied for each composite. The results are summarized in Table 2. The average pore sizes are of the same order of magnitude. The mercerized sample has the finest pore size distribution.

4.2 Cement-based materials

Figure 10 shows the variation of the thermal conductivity of each of the concretes versus pressure and the adjustment to the serial-parallel model. A good representation of the data by the model can be seen in both cases.

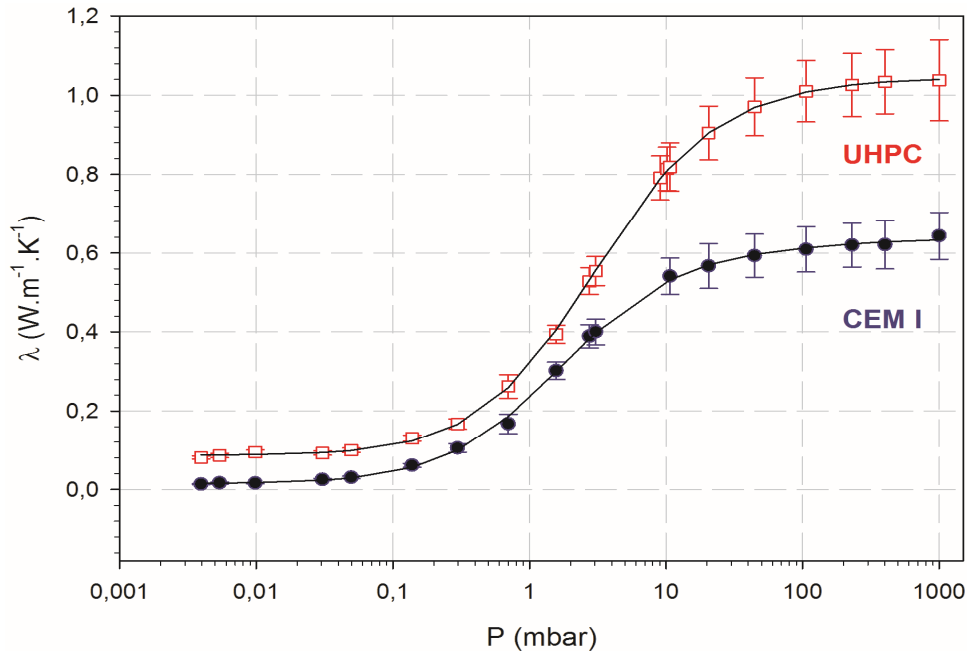


Figure 10. Variation of the thermal conductivity as a function of the pressure of two cement-based materials: CEM I, UHPC. (adjustment with serial/parallel model).

Pore size distribution of each of these materials is shown in Figures 11 and 12. In figure 11, it can be seen that the UHPC has a unimodal distribution of pore sizes around a few microns ($\sim 20 \mu\text{m}$). Normal law modeling gives an average size of $16 \mu\text{m}$ with a standard deviation of $0.3 \mu\text{m}$. Figure 12 shows that the CEM I has two distinct pore sizes, one around $20 \mu\text{m}$ and another, smaller, around 500 nm . The narrowest pore size can be seen on the experimental curve as near the atmospheric pressure, the thermal conductivity of the CEM I continues to increase however it stabilizes more for the UHPC. It should be noted that on this pressure range, smallest pores ($\sim 100 \text{ nm}$) affects mainly the conductivity (Figure 2).

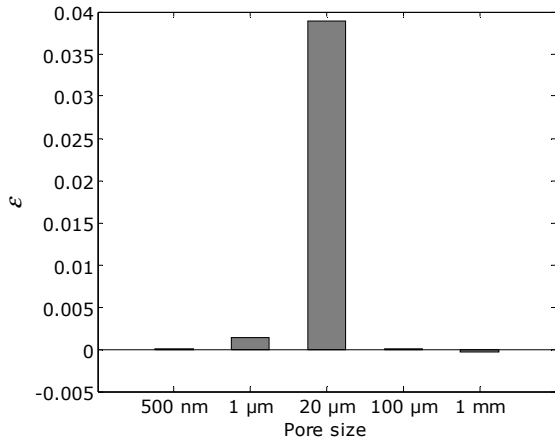


Figure 11. Estimation of the pore size distribution of the UHPC using the serial-parallel model.

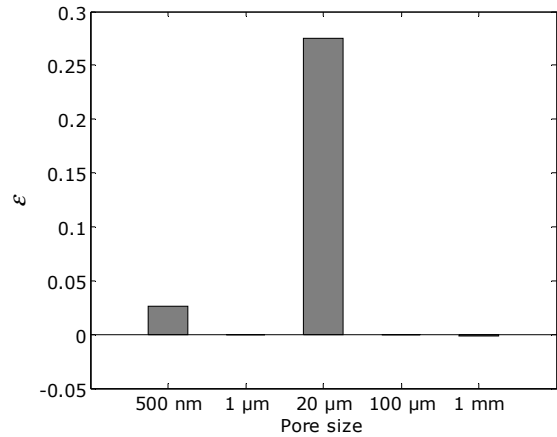


Figure 12. Estimation of the pore size distribution of the CEM I using the serial-parallel model.

Cement mortars and concrete have three categories of pores [32]. The largest pores are air bubbles ranging from a few microns to a millimeter. Intermediate pores are capillary pores that typically range from 10 nm to a few microns. The finest pores are the pores internal to the hydrates which are of nanometric size [33]. It should be noticed that each category of pore can be different according to the authors [34].

Experimentally, we observe that the two concretes have a similar pore range of about 20 μm. These pores could therefore correspond to the first category. This category is dominant, contrary to what is generally observed by mercury porosimetry but consistent with other techniques such as quantitative microscopy [34]. In addition, the CEM I has a finer pore size (~ 500 nm), which is not observed for the UHPC. This class of pores could correspond to capillary pores [32]. These would be absent from the UHPC, which illustrates perfectly that the UHPC is a concrete with very low capillary porosity [34]. However, the technique used does not allow to discretize more finely around a few nanometers. The limitations are related to the accessible pore size range and to the porosities which are of different nature (capillary and hydrate) and of similar sizes.

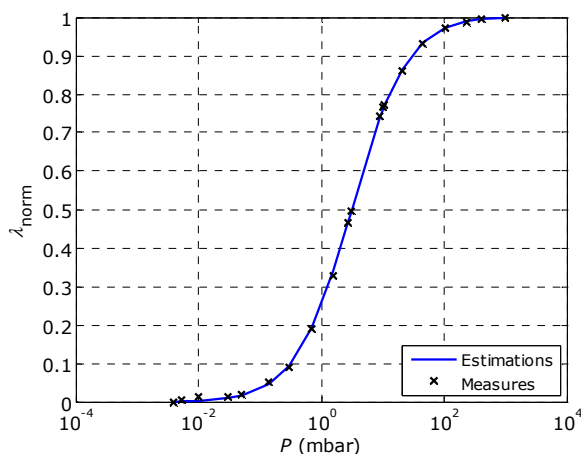


Figure 13. Comparison of measured and

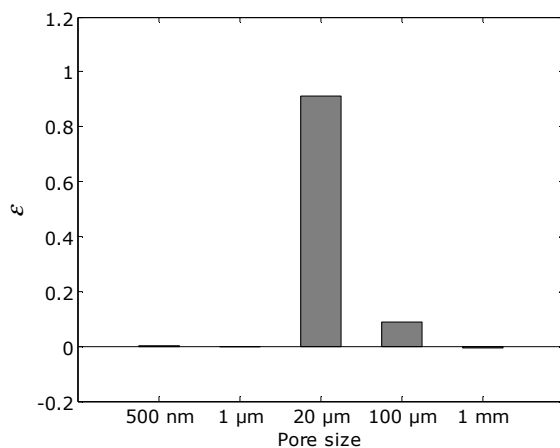


Figure 14. Estimation of the pore size

estimated normalized thermal conductivities
for the UHPC.

distribution of the UHPC using the
standardized serial-parallel model.

To overcome the overall porosity rate – which can vary by a factor of one to two [16] – it is possible to normalize the thermal conductivity (Figure 13). The serial-parallel model perfectly adjusts the normalized conductivity. The estimation of the pore sizes using this model is given in Figure 14. Compared with Figure 11, a slight increase in pore size is observed. The application of the normal distribution gives an average size of 24 μm and a standard deviation of 6.8 μm .

5. Conclusions

In this paper, we are interested in the pore size distribution of building materials. Contrary to most of the usual techniques, we propose a non-destructive technique, which takes into account the whole thickness of a specimen. This method is based on the modeling of the effective thermal conductivity of a material. Since the variation of the effective thermal conductivity is dependent on the pore size, this is a means of determining them. Based on the work of Félix *et al.* [11] which considers a heterogeneous media as N fluid phases and one solid phase in serial-parallel, we propose several extensions.

First of all, we show that this model and its extensions have been successfully applied to different insulation materials: natural fiber composites and cements. The transposition of the model from highly porous materials ($\sim 90\%$, [11]) to low porous materials (4-30 %) is conclusive. Secondly, we show that in the case of a single pore size it is possible to obtain a finer distribution based on a normal law. The thermal approach shows that the fiber reinforced composites have mainly one class of pores (30-60 μm). Chemical treatments of fibers only slightly affect this pore size. As far as cements based materials are concerned, they show a macroporosity (around 20 μm) which is often underestimated. This alternative thermal approach is also sensitive to capillary pores (100 nm) in cements but it is difficult to obtain a distribution of it. At last, by normalizing the effective thermal conductivity, we show for the first time that the determination of the pore size distribution is possible without the knowledge of the overall porosity rate. This improvement cannot be neglected since the determination of this parameter strongly depends on the technique used.

As an outlook towards further research, it could be interested to modify the current DICO device so as to reach pressure above the atmospheric one. This should allow to be sensitive to smaller pores (nanometrics) which could be relevant for discriminating capillary pores in cements or studying porosity in elementary fibers.

Acknowledgment:

The authors would like to thank Dr Poilane from the CIMAP laboratory for composite samples and EDE innov enterprise for cement samples.

References

- [1] A. Ciliberto, G. Cavaccini, O. Salvetti, M. Chimenti, L. Azzarelli, P.G. Bison, S. Marinetti, A. Freda, E. Grinzato, Porosity detection in composite aeronautical structures, *Infrared Physics and Technology*, 43 (2002) 139-143.
- [2] M.R. Hall, *Materials for Energy Efficiency and Thermal Comfort in Buildings* ISBN: 978-1-84569-526-2, 2010, Woodhead Publishing, 760
- [3] S. Diamond, An inappropriate method for the measurement of pore size distributions in cement based materials, *Cement and Concrete Research*, V30, 10 (2000) 1517-1525
- [4] S. Diamond, Aspects of concrete porosity revised, *Cement and Concrete Research*, 29 (1999)1181-1188.
- [5] I. C. Micrometrics, Auto pore IV 9500, Part no.950-42801-01, 2000.
- [6] R. Gerhardt, A review of conventional and non-conventional pore characterization techniques, *Mater. Res. Soc. Symposium Proceedings*, 137, Pore Structure and Permeability of Cementitious Materials (1989) 75-82.
- [7] K. K. Aligizaki, *Pore structure of cement-based materials: testing, interpretation and requirements*, 2006.
- [8] M. M. Canut, *Pore structure in blended cement pastes*, PhD, Thesis, Department of Civil Engineering Technical University of Denmark, 2011.
- [9] P. J. McDonald, J. M. Mitchell, M. M. Mulheron, *Cement Products: Characterisation by NMR and MRI*, School of Electronics and Physical Sciences, and School of Engineering University of Surrey Guildford (2005) 1-33.
- [10] Z. Sun, G. W. Scherer, Pore size and shape in mortar by thermoporometry, *Cement and Concrete Research* 40 (2010) 740-751.
- [11] V. Félix, Y. Jannot, A. Degiovanni, A thermal porosimetry method to estimate pore size distribution in highly porous insulating materials, *Review of scientific Instruments* 83 (2012) 054903
- [12] M.P. Connolly, The measurement of porosity in composite materials using infrared thermography, *Journal of reinforced plastics and composites*, 11-12 (1992) 1367-1375
- [13] V. Feuillet, N. Dujardin, M. Fois, L. Ibos, C. Poilâne, and Y. Candau, Pulsed thermography: a useful tool to determine porosity in composite materials?, in *11th International Conference on Quantitative InfraRed Thermography*, Naples, Italy, 11–14 (2012).
- [14] M.A. Aegerter et al. (eds.), *AerogelsHandbook, Advances in Sol-Gel Derived Materials and Technologies*, DOI 10.1007/978-1-4419-7589-8_42 (2011), ch23 Hans-Peter Ebert.

- [15] C. Li, B. Li, N. Pan, Z. Chen, M. Umar Saeed, T. Xu, Y. Yang, Thermo-physical properties of polyester fiber reinforced fumed silica/hollow glass microsphere composite core and resulted vacuum insulation panel, *Energy and Buildings*, 125 (2016) 298-309
- [16] T. Tracz, Open porosity of cement pastes and their gas permeability, *Bul. Pol. Ac. Tech.*, 64-4 (2016) 775-783
- [17] A. Boudenne, L. Ibos, E. Gehin, Y. Candau, A simultaneous characterization of thermal conductivity and diffusivity of polymer materials by a periodic method, *Journal of Physics D: Applied Physics*, 37-1 (2004) 132-139
- [18] Z.E. Cherif, C. Poilâne, A. Vivet, B. Ben Doudou, J.Chen, About optimal architecture of plant fibre textile composite for mechanical and sorption properties, *Composite Structures*, 140 (2016) 240-251
- [19] L. J. Parrot, W. Hansen, R. L. Berger, Effect of first drying upon the pore structure of hydrated alite paste, *Cement and Concrete Research*, 10 (1980) 647-655
- [20] D. H. Bager, E. J. Sellevold, Ice formation in hardened cement paste, Part II – drying and resaturation on room temperature cured pastes, *Cement and Concrete Research*, 16 (1986) 835-844
- [21] A. Korpa, R. Trettin, The influence of different drying methods on cement paste microstructures as reflected by gas adsorption: Comparison between freeze-drying (F drying), D-drying, P-drying and oven-drying methods, *Cement and Concrete Research*, 36 (2006) 634-649
- [22] R. M. Espinosa, L. Franke, Influence of the age and drying process on pore structure and sorption isotherms of hardened cement paste, *Cement and Concrete Research*, 36 (2006) 1969-1984
- [23] L. Ibos, R. Tlili, A. Boudenne, M. Fois, N. Dujardin, Y. Candau, Thermophysical characterization of polymers according to the temperature using a periodic method. *Polymer Testing* 66 (2018) 235–243
- [24] P. G. Collishaw, J. R. G. Evans, An assessment of expressions for the apparent thermal conductivity of cellular materials, *Journal of Materials Science* 29 (1994) 2261-2273
- [25] Y. Jannot, A. Degiovanni, M. Camus, Extension of the thermal porosimetry method to high gas pressure for nanoporosimetry estimation, *Review of scientific instruments*, 89 (2018), 044904
- [26] D. W. Marquardt, An algorithm for the least squares estimation of non linear parameters, *SIAM Journal*, 1 (1963) 431-441
- [27] Z. Mahboob, H. Bougherara, Fatigue of flax-epoxy and other plant fibre composites: Critical review and analysis, *Composites Part A: Applied Science and Manufacturing*, 109 (2018) 440-462.

- [28] B. Madsen, H. Lilholt, Physical and mechanical properties of unidirectional plant fibre composites-an evaluation of the influence of porosity, *Composites Science and Technology*, 63-9 (2003) 1265-1272.
- [29] B. Madsen, A. Thygesen, H. Lilholt, Plant fibre composites – porosity and volumetric interaction, *Composites Science and Technology*, 67-7–8 (2007) 1584-1600.
- [30] B. Madsen, A. Thygesen, H. Lilholt, Plant fibre composites – porosity and stiffness, *Composites Science and Technology*, 69-7 (2009) 1057-1069.
- [31] R. Kumar, B. Bhattacharjee, Porosity, pore size distribution and in situ strength of concrete, *Cement and Concrete Research* 33 (2003) 155–164.
- [32] K. Charlet, C. Morvan, J. Brérad, J.P. Jernot, M. Gomina, Etude morphologique d'un composite naturel La fibre de lin, *Revue des composites et des matériaux avancés*, 16-1 (2006) 11-24.
- [33] A.C.A. Muller, Characterization of porosity & C-S-H in cement pastes by ¹H NMR, PhD Thesis, Ecole polytechnique fédérale de Lausanne (2014).
- [34] J.D. Birchall, A.J. Howard, K. Kendall, Flexural strength and porosity of cements, *Nature*, 289 (1981) 388-390.